Journal of Integrative Neuroscience

J. Integr. Neurosci. **2026**; 25(3): 49920
https://doi.org/10.31083/JIN49920

Original Research

Whole-Body Vibration Promotes Neurological Recovery From Subarachnoid Hemorrhage via Meningeal Lymphatic Drainage and CD4$^+$ Treg-Mediated Immunomodulation

Cui-Yun Sun[1,†], Yan-Yu Zang[1,†], Xiao-Cong Su[2,†], Jing-Wen Chen[3], Shuai-Fei Lu[3], Xiao-Jian Li[4], Xiao-Yu Teng[2,*], Yun Stone Shi[2,3,*], Rong Xu[1,*]

[1]Department of Rehabilitation Medicine, Nanjing Drum Tower Hospital, Affiliated Hospital of Medical School, Nanjing University, 210008 Nanjing, Jiangsu, China
[2]Guangdong Institute of Intelligence Science and Technology, 519031 Zhuhai, Guangdong, China
[3]Ministry of Education Key Laboratory of Model Animal for Disease Study, Model Animal Research Center, National Resource Center for Mutant Mice, Medical School, Nanjing University, 210032 Nanjing, Jiangsu, China
[4]Department of Neurosurgery, Nanjing Drum Tower Hospital, Affiliated Hospital of Medical School, Nanjing University, 210008 Nanjing, Jiangsu, China
*Correspondence: tengxiaoyu@smail.nju.edu.cn (Xiao-Yu Teng); yunshi@nju.edu.cn (Yun Stone Shi); xurong3973@163.com (Rong Xu)
†These authors contributed equally.
Academic Editor: Moo-Ho Won
Submitted: 12 January 2026 Revised: 9 February 2026 Accepted: 24 February 2026 Published: 18 March 2026

Abstract

Background: Whole-body vibration (WBV) has emerged as a promising non-pharmacological intervention for chronic neurological disorders; however, its underlying mechanisms remain incompletely understood. In this study, we investigated the therapeutic efficacy and mechanistic basis of WBV in subarachnoid hemorrhage (SAH), a severe condition characterized by high mortality and long-term neurological deficits. **Methods**: SAH was induced in mice via chiasmatic cistern injection. WBV intervention (frequency: 28 Hz, amplitude: 0.3 mm) was initiated 7 days post-SAH and continued for 3 consecutive weeks. Neurological function was assessed using the open field test, Morris water maze, Y-maze, and gait analysis. Meningeal lymphatic vessel (MLV)-mediated drainage was evaluated through *in vivo* fluorescence imaging of Evans blue and Alexa Fluor 647-conjugated ovalbumin clearance. The expression of podoplanin (*Pdpn*) and lymphatic vessel endothelial hyaluronan receptor 1 (*Lyve-1*), specific markers of meningeal lymphatic endothelial cells, was analyzed in MLVs and deep cervical lymph nodes (dCLNs) using quantitative real-time polymerase chain reaction (qRT-PCR). Peripheral immunomodulatory changes were assessed by quantifying cluster of differentiation 4 and forkhead box protein P3 positive (CD4$^+$Foxp3$^+$) regulatory T cells (Tregs) in peripheral blood mononuclear cells via flow cytometry. **Results**: WBV treatment significantly improved learning and memory deficits, emotional disturbances, and motor dysfunction in SAH mice. Mechanistically, WBV enhanced the drainage capacity of MLVs by promoting lymphangiogenesis. Furthermore, WBV increased the proportion of peripheral Tregs, indicating an enhanced immunomodulatory effect. **Conclusions**: This study demonstrates that WBV facilitates neurological recovery post-SAH by enhancing meningeal lymphatic drainage and expanding the peripheral Treg population. These findings highlight WBV as a promising, non-invasive therapeutic strategy for SAH rehabilitation.

Keywords: subarachnoid hemorrhage; vibration; meningeal lymphatic vessel; lymphangiogenesis; regulatory T cells

1. Introduction

Subarachnoid hemorrhage (SAH), primarily resulting from ruptured intracranial aneurysm, is a life-threatening cerebrovascular event and the second leading cause of stroke-related mortality [1,2]. Early brain injury typically occurs within the first three days post-hemorrhage, followed by delayed cerebral ischemia developing three to four days later [3]. Approximately 50% of patients die from the initial hemorrhage, while an additional 30% of survivors develop delayed neurological deficits that severely compromise their quality of life [4]. Long-term neurological deficits often include cognitive and emotional impairments, with memory dysfunction affecting 50–60% of SAH survivors [5]. The inflammatory response mediated by immune cells represents a critical physiological reaction that contributes to secondary brain injury [6].

The recent discovery of meningeal lymphatic vessels (MLVs) and glymphatic pathways has overturned the long-standing belief that the central nervous system (CNS) lacks a lymphatic system. MLVs drain cerebrospinal fluid (CSF) and metabolic waste from the brain into cervical lymph nodes (CLNs), playing a crucial role in neuroimmune regulation [7,8]. In cerebrovascular diseases, MLVs exhibit plasticity, and their dysfunction contributes to neuropathological progression [9]. Recent studies demonstrated that MLVs are key in clearing erythrocytes from hemorrhage and other macromolecular solutes [10–12]. Impairment of MLVs exacerbates early brain injury in experimental SAH

[13]. Pharmacological agents such as ketoprofen, 9-cis retinoic acid (9-cisRA), and vascular endothelial growth factor C (VEGF-C) enhance MLV integrity and function in traumatic brain injury models [14]. Furthermore, MLVs facilitate the drainage of immune cells from the CNS into deep cervical lymph nodes (dCLNs). Enhancing the clearance of T helper 17 (Th17) cells via MLVs alleviates neuroinflammation after SAH [15], suggesting that targeting lymphatic drainage pathways represents a promising therapeutic strategy.

Whole-body vibration (WBV) is an effective intervention for improving body composition, muscle strength, postural stability, bone mass, sensorimotor performance, and cardiovascular function [16]. Recently, WBV has gained attention as a non-invasive therapeutic approach for neurological disorders, such as Alzheimer's Disease (AD) [17,18]. Murine studies indicate that WBV stimulates neurogenesis, enhances neuronal plasticity, and influences neurotransmitter transmission [19,20]. Clinical evidence also supports its potential in rehabilitating Parkinson's disease and enhancing cognitive [21,22]. Moreover, WBV modulates inflammatory responses through mechanosensory stimulation [23]. However, its neuroprotective mechanisms, particularly following SAH, remain poorly understood.

This study investigated the efficacy of a three-week WBV intervention in a mouse model of SAH, focusing on its effects on neurological function, meningeal lymphatic drainage, and peripheral immunomodulation. Our findings aim to elucidate the potential mechanisms underlying WBV as a rehabilitative strategy for SAH.

2. Materials and Methods

2.1 Animals

Male C57BL/6J mice (8 weeks old, 22–25 g) were purchased from GemPharmatech Co., Ltd. (Nanjing, Jiangsu, China) and housed under specific pathogen-free (SPF) conditions with ad libitum access to standard rodent chow and water. Animals were maintained in a controlled environment at 25 $\pm$ 1 °C and 65 $\pm$ 5% relative humidity, under a 12-h light/dark cycle. The mice were assigned to one of three conditions: (i) sham operation (sham), (ii) SAH induction alone (SAH), or (iii) SAH induction followed by WBV treatment (SAH-WBV).

2.2 SAH Model Induction and dCLN Ligation

The SAH model was induced via chiasmatic cistern injection as previously described [24]. Briefly, mice were anesthetized with 5% isoflurane and maintained on 1.5% isoflurane (R510-22-10, RWD, Shenzhen, Guangdong, China) during surgery. Donor mice were positioned supinely, and their thoracic skin was disinfected. Arterial blood was obtained via cardiac puncture of the left ventricle using an insulin syringe. Donor mice were then euthanized by cervical dislocation. Experimental mice were anesthetized, positioned prone in a stereotaxic apparatus, and the scalp was disinfected and incised to expose the anterior fontanelle. A 1 mm diameter hole was drilled approximately 4.5 mm anterior to the fontanelle and 2 mm lateral to the midline. An insulin needle containing donor blood was inserted at a 45-degree angle to a depth of ~4 mm, and 50 µL of arterial blood was slowly injected. The needle was left in place for 2 min prior to its removal, and the skull hole was sealed with bone wax. The surgical area was sterilized, and the skin was sutured. Sham group mice underwent the same procedure without blood injection. All mice recovered in a temperature-controlled environment. For the ligation group, a neck incision exposed the trachea, and the left dCLN was ligated. The control group had dCLN exposure without ligation.

2.3 Modified Garcia Neurological Scoring Test

SAH severity was evaluated 24 h post-SAH using a grading scale. The scale assesses six behavioral domains (spontaneous activity, symmetric limb movement, forelimb extension, vertical climbing, trunk touch response, vibrissae tactile sensation), each scored from 0 to 3. Total scores range from 0 to 18. An independent researcher performed all tests and grading. SAH model mice scoring $\leq$9 were excluded based on validated criteria.

2.4 WBV Intervention

WBV intervention was administered using a commercial platform (Thermo Cyclo Pad, Model TCP-2021; Niagara Medical, Brisbane, Australia). The parameter was set to a frequency of 28 Hz and a peak-to-peak displacement amplitude of 0.3 mm. Before each session, mice underwent 30-min environmental acclimatization. During WBV, SAH and sham groups were individually housed in ventilated plexiglass chambers (10 $\times$ 10 $\times$ 15 cm) mounted on the platform to standardize posture and restrict locomotion. The SAH-WBV group received continuous vertical sinusoidal vibrations, while the SAH group was placed on an inactive platform. This protocol was administered once daily for 3 consecutive weeks, starting 7 days post-surgery, at consistent circadian times.

2.5 Open Field Test

Spontaneous activity and anxiety-like behaviors were assessed using an open field apparatus (Model: ZH-SBS Type; Anhui Zhenghua Biological Instrument Equipment Co., Ltd., Huaibei, Anhui, China). Mice freely explored in a blue box (50 $\times$ 50 $\times$ 25 cm) with a defined central zone (20 $\times$ 20 cm). Each mouse was placed in the center and allowed to explore for 5 min. Total distance moved and time spent in the central zone were automatically tracked. The arena was cleaned with 70% ethanol between trials. Data were analyzed using the ZH-SBS Animal Fine Behavior Analysis System (v2.01, Anhui Zhenghua Biological Instrument Equipment Co., Ltd.).

2.6 Y-maze Test

Spatial working memory was evaluated using a standardized Y maze with three identical opaque arms (35 × 10 × 15 cm) arranged at 120°. Each mouse was placed in the central hub under 50 lux illumination and allowed to explore freely for 8 min. Spontaneous alternation was defined as consecutive entries into three distinct arms without repetition. Mice with fewer than 8 total arm entries were excluded. Sessions were recorded and analyzed using the ZH-SBS Animal Fine Behavior Analysis System, with arm entry defined as ≥90% body displacement into an arm.

2.7 Morris Water Maze Test

The Morris water maze protocol included a 6-day acquisition phase and a probe trial. During acquisition (Days 1–5), mice underwent four trials/day (30-min inter-trial interval) in a circular pool (120 cm diameter, 50 cm height, 22 ± 1 °C water) containing a hidden platform (10 cm diameter) positioned 1 cm below the water surface in the target quadrant. Spatial cues surrounded the pool. Each trial lasted up to 60 s; mice finding the platform remained for 15 s, while others were guided to it. On Day 6, the platform was removed for a 60-second probe trial. Data, including the time spent in the target quadrant and the number of crossings of the platform area, were recorded. Data were analyzed via the ZH-SBS Animal Fine Behavior Analysis System.

2.8 Gait Analysis

Gait analysis was performed using the CatWalk XT 10.6 system (Noldus Information Technology, Wageningen, Netherlands). Mice were acclimatized for 15–20 min before testing. Each mouse was placed on a 1.1 m glass walkway under dim lighting (15 lux), with paw contacts visualized via total internal reflection of 532 nm green light. A high-speed CMOS camera (FASTCAM Mini UX100, Photron, San Diego, CA, USA) recorded paw prints at 100 Hz. Animals completed a 7-day acclimatization protocol with three daily trials (5–10 min/trial, ≥2 h inter-trial interval) before formal testing. Gait parameters were extracted using manufacturer software (run speed variation threshold <60%, complete step sequence required). Analyzed metrics included spatiotemporal parameters (stride length, stance duration, swing speed), dynamic parameters (print area, maximum contact pressure), and interlimb coordination (regularity index, phase dispersion). Raw data and intensity profiles were exported for analysis.

2.9 H&E and Nissl Staining

Mice were deeply anesthetized with avertin (240 mg/kg, intraperitoneal injection, DW3101, Dowobio, Shanghai, China) and transcardially perfused with 50 mL ice-cold phosphate-buffered saline (PBS) followed by 50 mL 4% paraformaldehyde (A500684-0500, Sangon Biotech, Shanghai, China). Brains were dissected and post-fixed at 4 °C for 24 h. Tissues were dehydrated through a graded ethanol series (70%–80%–90%–100%, 1 h each), cleared in xylene (10023418, Sinopharm, Shanghai, China), and embedded in paraffin (39601095, Leica, Richmond, IL, USA). Serial coronal sections (5 µm thick) were cut using a rotary microtome (RM2235, Leica). For hematoxylin and eosin (H&E) staining, deparaffinized sections were stained with Mayer's hematoxylin (SL7050, Coolaber, Beijing, China) for 5 min, differentiated in 1% acid alcohol, rinsed in tap water, counterstained with eosin Y (SL7060, Coolaber) for 2 min, dehydrated, cleared, and mounted with neutral balsam (G8590, Solarbio, Beijing, China). For Nissl staining [25], sections were incubated in 0.1% cresyl violet (C9140, Solarbio) at 50 °C for 10 min, differentiated in 95% ethanol with 0.1% acetic acid (10000218, Sinopharm), dehydrated, cleared, and coverslipped with distyrene plasticizer xylene (DPX, MM1410, MKBio, Shanghai, China). Sections were imaged under bright-field illumination using a Leica microscope (DM2500, Leica) with a 20×/0.7 NA objective lens and a DFC450 CCD camera.

2.10 Quantitative Real-Time Polymerase Chain Reaction (qRT-PCR)

Total RNA was isolated from dura mater using RNAiso™ Plus reagent (9109, TAKARA, Kyoto, Japan). First-strand cDNA was synthesized from 1 µg total RNA using HiScript® II Q RT SuperMix (R223-01, Vazyme, Nanjing, Jiangsu, China). qPCR was performed using NovoStart® Universal Fast SYBR qPCR SuperMix (E401-01A, Novoprotein, Shanghai, China) on a QuantStudio™ 6 Pro system (Applied Biosystems, Carlsbad, CA, USA). Reactions were run in triplicate under: 95 °C for 30 s, 40 cycles of 95 °C for 10 s, and 60 °C for 30 s. Gene expression was normalized to *Gapdh* and calculated via the $2^{-\Delta\Delta Ct}$ method. Primers were designed via PrimerBank (https://pga.mgh.harvard.edu/primerbank/) and synthesized by GenScript Biotech Co., Ltd. (Nanjing, Jiangsu, China). Primer sequences (5′-3′) were as follows: *Gapdh* (NM_001289726.2): Forward: AGGTCGGTGTGAACGGATTTG; Reverse: GGGGTCGTTGATGGCAACA (size: 95 bp). Podoplanin (*Pdpn*, NM_001290822.2): Forward: GTTTTGGGGAGCGTTTGGTTC; Reverse: CATTAAGCCCTCCAGTAGCAC (size: 154 bp). Lymphatic vessel endothelial hyaluronan receptor 1 (*Lyve-1*, NM_053247.4): Forward: CAGCACACTAGCCTGGTGTTA; Reverse: GGAAAGGTCTTGCACGAGGTC (size: 87 bp).

2.11 Western Blot

The tissues were homogenized in chilled RIPA lysis buffer (KGB5204-100, KeyGEN Biotech, Nanjing, Jiangsu, China) for 5 min using a homogenizer (F6/10, Jingxin, Shanghai, China). Subsequently, the homogenate was centrifuged at 12,000 rpm for 10 min at 4 °C, and

the supernatant was transferred to a clean 1.5 mL tube (CFT801015, Jet Biofil, Guangzhou, Guangdong, China). After running sodium dodecyl sulfate-polyacrylamide gel electrophoresis (SDS-PAGE) gels (ET10010LGel, ACE, Changzhou, Jiangsu, China) in an ice-cold buffer, the proteins were transferred onto a PVDF membrane (WJ002, EpiZyme, Shanghai, China). Immunoblots were probed with the indicated antibodies. The primary antibodies include: Syrian hamster anti-PDPN (1:300, ab11936, Abcam, Cambridge, UK), rabbit anti-LYVE-1 (1:500, ab14917, Abcam), and rabbit anti-GAPDH (1:3000, B8016, Biodragon, Suzhou, Jiangsu, China).

2.12 Immunofluorescence Staining

For immunofluorescence staining, the tissue sections were blocked with a solution containing 5% bovine serum albumin (BSA, HYB780, HUAYUN, Guangzhou, Guangdong, China) and 0.3% Triton X-100 (A110694-0100, Sangon Biotech) for 1 h at room temperature (RT). Subsequently, they were incubated sequentially: first with the primary antibody overnight at 4 °C, followed by incubation with a fluorescent-dye-conjugated secondary antibody for 1 h at RT. The primary antibody used in this study was rabbit anti-LYVE-1 (1:500, ab14917, Abcam). The appropriate Alexa Fluor-conjugated secondary antibody was a donkey anti-rabbit antibody (1:1000, abs20021, Absin, Shanghai, China). The nuclei were counterstained with 4′,6-diamidino-2-phenylindole (DAPI, C1002, Beyotime, Shanghai, China) at RT. Fluorescent images were captured using a confocal laser-scanning microscope (LSM880, Zeiss, Oberkochen, Germany).

2.13 Intracerebroventricular Injection (i.c.v.) and In Vivo Optical Imaging

Mice were anesthetized with 5% isoflurane in 100% oxygen (1 L/min) and secured in a digital stereotaxic frame (68811, RWD) with 2% isoflurane during imaging. The dorsal cervical skin was shaved and aseptically prepared. Ocular lubrication (19-7223, HOYON, Shenzhen, Guangdong, China) was applied. After a midline incision exposed the calvaria, bregma coordinates were zeroed. The left lateral ventricle was targeted (AP –0.35 mm, ML +1.0 mm, DV –2.3 mm). In different experiments, either Evans Blue (EB, 10% w/v, A602025-0005, Sangon Biotech) or Alexa Fluor 647-conjugated ovalbumin (OVA-647, O34784, Invitrogen, Carlsbad, CA, USA) was injected using a microinjection pump at a rate of 0.2 µL/min. The needle remained in place for 5 min post-injection. EB fluorescence was imaged 4 h post-SAH, and OVA-647 fluorescence was imaged 12 h post-injection using an IVIS® Lumina Series III (PerkinElmer, Waltham, MA, USA). Radiant efficiency was analyzed.

2.14 Flow Cytometry Analysis

Peripheral blood mononuclear cells (PBMCs) were isolated via density gradient centrifugation (725431, NEST Biotechnology, Wuxi, Jiangsu, China). For surface staining, cells were incubated with an FITC-conjugated anti-cluster of differentiation 4 (CD4) antibody (clone RM4-5, 11-0042-82, eBioscience, San Diego, CA, USA; 1:100, 30 min, 4 °C). Cells were washed with PBS, then fixed/permeabilized using the Forkhead box protein P3 (Foxp3)/Transcription Factor Staining Buffer Set (00-5523-00, eBioscience). Intracellular staining used anti-Foxp3 PE (clone FJK-16s, 12-5773-82, eBioscience; 60 min, 4 °C, dark). Data were acquired on a BD FACSAria™ III with FACSDiva™ software (v8.0.1, BD Biosciences, Franklin Lakes, NJ, USA), collecting $\geq$5000 events in the lymphocyte gate. Tregs were defined as $CD4^+/Foxp3^+$ population. Data were analyzed using FlowJo™ (v10.8.1, Agilent, Santa Clara, CA, USA).

2.15 Statistics

Analyses were conducted in GraphPad Prism (Version 10.0.2, GraphPad Software, San Diego, CA, USA). Normality was assessed via Shapiro-Wilk tests ($\alpha = 0.05$); homogeneity of variance was confirmed by Brown-Forsythe tests. Multi-group comparisons meeting parametric assumptions used one-way ANOVA with Tukey's post hoc test. Non-normal data used Kruskal-Wallis test with Dunn's correction. Continuous variables are expressed as mean $\pm$ SEM, with n values indicated in figure legends. Significance was set at $p < 0.05$ (*$p < 0.05$, **$p < 0.01$, ***$p < 0.001$, and ****$p < 0.0001$).

3. Results

3.1 WBV Alleviates SAH-Induced Cognitive and Affective Deficits

The SAH model was established via chiasmatic cistern injection, and the long-term effects of WBV in mice following SAH were examined (Fig. 1A). Within 1 h post-injection, visible blood accumulation in basal cisterns was observed in the SAH group but not in sham controls (Fig. 1B). Neurological function assessed 24 h post-SAH via the Modified Garcia test showed no significant score differences between SAH and sham groups (Fig. 1C). Motor coordination assessed via the beam walking test revealed significantly prolonged traversal times in SAH mice compared to sham controls (Fig. 1D). H&E staining revealed cerebral edema and dilated perivascular spaces in the cortex and hippocampus of SAH mice (Fig. 1E). WBV treatment was initiated 7 days after SAH induction and administered using a vertical sinusoidal vibration platform operating at a frequency of 28 Hz and an amplitude of 0.3 mm (Fig. 1F). SAH-WBV mice received daily 30-min sessions for 21 consecutive days; control SAH mice were placed on an inactive platform. Open field, Y-maze, and Morris water maze tasks were conducted 3 weeks after WBV interven-

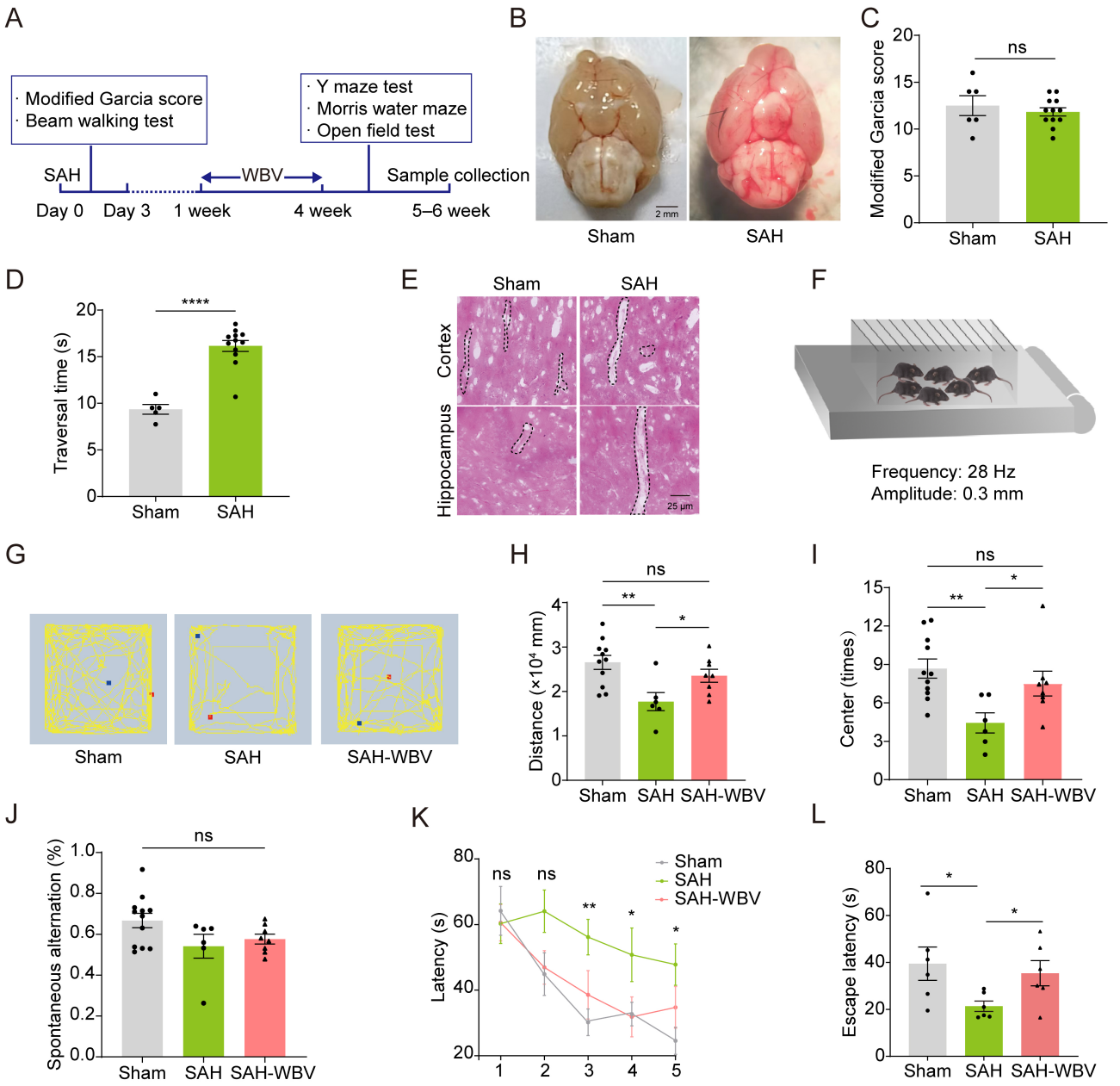

Fig. 1. WBV alleviates SAH-induced cognitive and affective deficits. (A) Experimental timeline. (B) Macroscopic brain morphology. Scale bar: 2 mm. (C) Modified Garcia score (sham, n = 6; SAH, n = 12). (D) The traversal time in the beam walking test (sham, n = 5; SAH, n = 12). (E) H&E staining for perivascular space pathology. Representative images from three replicates. Scale bar: 25 μm. (F) WBV parameters: frequency, 28 Hz; amplitude, 0.3 mm; 30 min/day for 21 days. (G–I) Open field test: [G], Representative locomotor activity graphic; [H], Total distance traveled; [I], Center zone dwell time (sham, n = 11; SAH, n = 6; SAH-WBV, n = 8). (J) Spontaneous alternation rate in the Y-maze test (sham, n = 12; SAH, n = 6; SAH-WBV, n = 8). (K,L) Morris water maze: K, Escape latency during acquisition; L, Probe trial latency (sham, n = 6; SAH, n = 6; SAH-WBV, n = 6). Abbreviations: SAH, subarachnoid hemorrhage; SAH-WBV, SAH mice treated with whole-body vibration; H&E, hematoxylin and eosin. Data are presented as mean ± SEM. ns, $p > 0.05$, *$p < 0.05$, **$p < 0.01$, ****$p < 0.0001$.

tion. The open field test revealed significant decreases in total distance moved and center time in SAH mice compared to sham controls (Fig. 1G–I), indicating impaired locomotion and anxiety-like behavior. WBV intervention effectively reversed these deficits (Fig. 1G–I). The Y-maze spontaneous alternation task showed no significant differences among groups (Fig. 1J). In the Morris water maze acquisition phase, SAH mice showed impaired spatial learning, with a slower reduction in escape latency across days compared to sham controls. Notably, SAH-WBV mice showed improved learning from days 3–5 (Fig. 1K). During the probe trial, SAH-WBV mice spent significantly more time

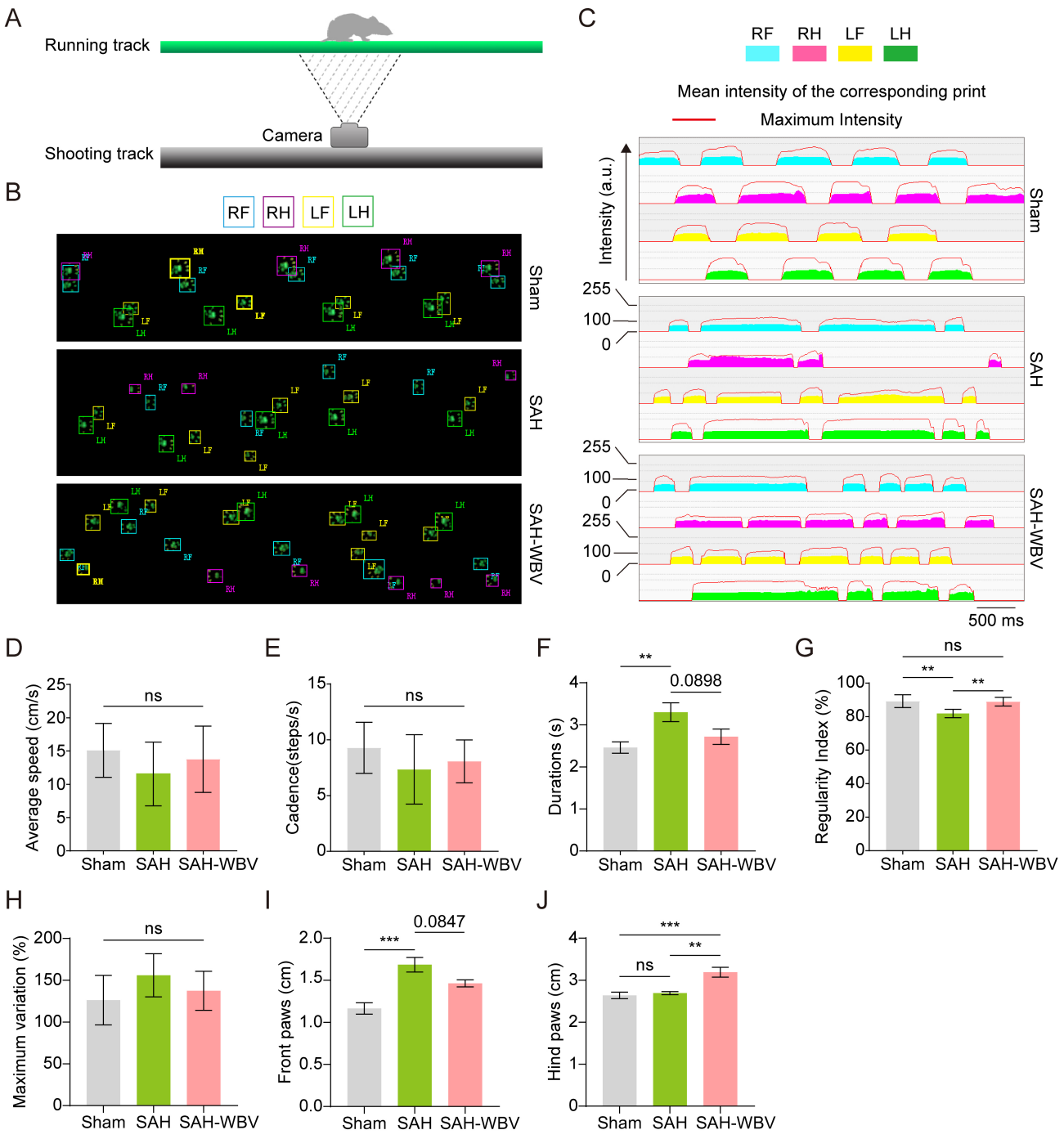

Fig. 2. WBV improves gait behavior in SAH mice. (A) CatWalk XT gait analysis. (B,C) Paw profiles: B, Raw grayscale prints; C, Heatmaps of paw intensity (a.u.) (n = 6 mice/group). (D–J) Statistical analysis of gait parameters: [D], Speed (cm/s); [E], Cadence (steps/s); [F], Run duration (s); [G], Regularity index (%); [H], Maximum variation (%); [I], Front paws (cm); [J], Hind paws (cm). Data are presented as mean ± SEM. Statistical significance: ns, $p > 0.05$, $^{**}p < 0.01$, $^{***}p < 0.001$. RF, right forelimb; RH, right hindlimb; LF, left forelimb; LH, left hindlimb.

in the target quadrant than the SAH group, indicating restored spatial memory (Fig. 1L). Collectively, these findings suggest that WBV therapy alleviates cognitive and affective deficits in SAH mice.

3.2 WBV Improves Gait Behavior in SAH Mice

To investigate the effect of WBV on gait in post-SAH mice, we performed gait analysis (Fig. 2A). Spatiotemporal parameters and dynamic parameters were recorded (Fig. 2B,C). Key gait features, including run duration, average speed, and regularity index, were analyzed. SAH sig-

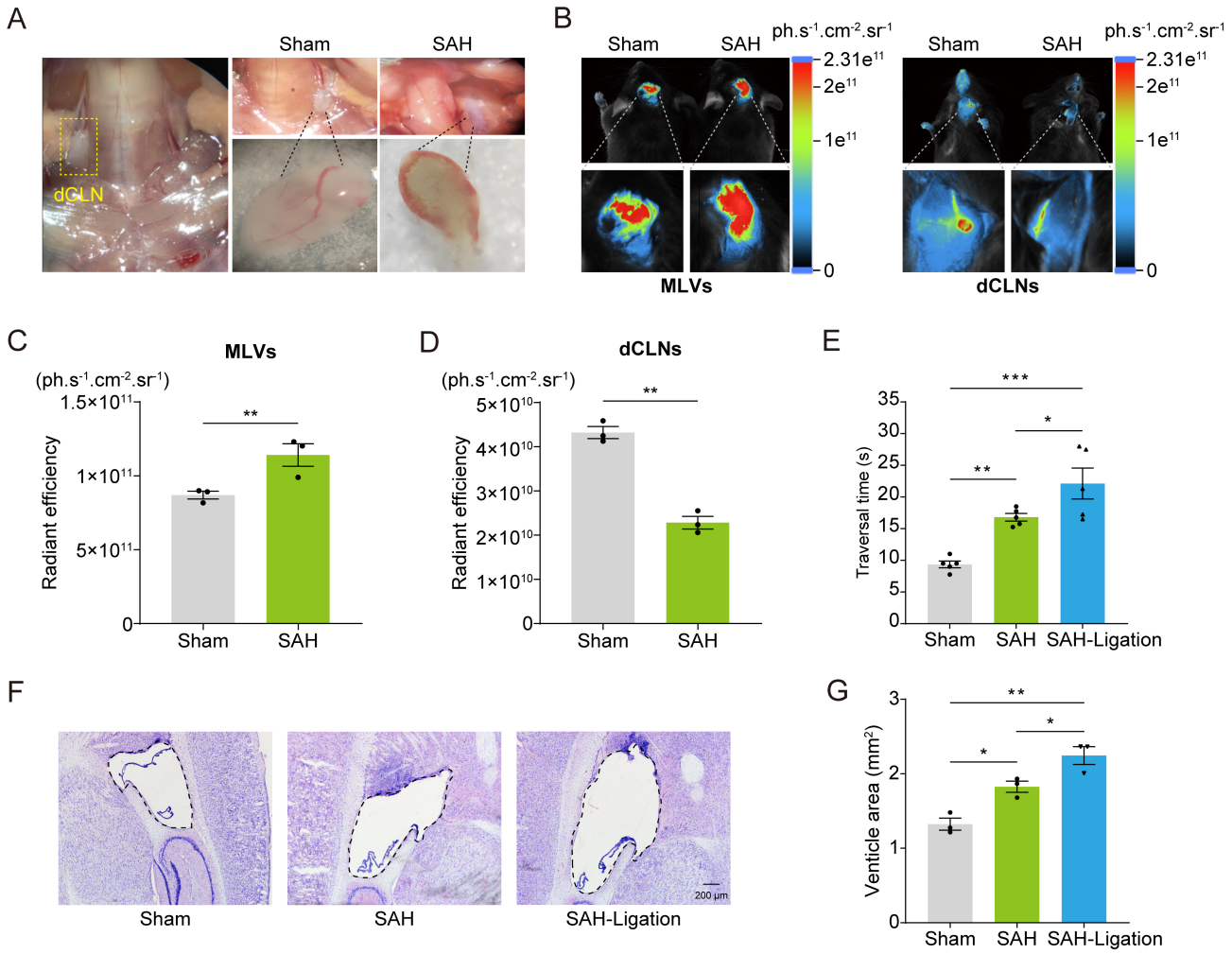

Fig. 3. SAH impairs meningeal lymphatic drainage. (A) Erythrocyte accumulation in dCLNs. (B) *In vivo* imaging of 2% Evans blue (5 μL) in MLVs and dCLNs after intracerebroventricular injection for 4 h. (C,D) Quantified fluorescence intensity in MLVs (C) and dCLNs (D) (n = 3 mice/group). (E) Traversal time in the beam walking test (n = 5 mice/group). (F) Nissl staining results. Scale bar: 200 μm. (G) Quantification of the lateral ventricle. Data are presented as mean ± SEM. Statistical significance: $*p < 0.05$, $**p < 0.01$, $***p < 0.001$. MLV, meningeal lymphatic vessel; dCLN, deep cervical lymph node.

nificantly altered run duration, regularity index, and front paw contact area. WBV treatment partially reversed these impairments, significantly improving the regularity index and hind paw contact area compared to the SAH group (Fig. 2D–J). Taken together, these findings indicate that WBV improves locomotor coordination and paw motor control in SAH mice.

3.3 SAH Impairs Meningeal Lymphatic Drainage

MLV drainage is critical for cerebral homeostasis [11]. To assess MLV-mediated blood clearance post-SAH, we examined dCLNs in sham and SAH mice. At 4 h post-injection, erythrocyte infiltration was observed in dCLNs of SAH mice, but not saline-injected controls (Fig. 3A). To evaluate MLV drainage efficacy, 2% Evans blue was injected into the lateral ventricle. *In vivo* imaging showed reduced fluorescence in dCLNs and increased fluorescence in MLVs of SAH mice compared to sham controls, indicating greater cerebral Evans blue retention (Fig. 3B–D). To further investigate the impact of lymphatic dysfunction on SAH progression, unilateral lymphatic ligation was performed 24 h pre-SAH. Beam walking performance and lateral ventricle area were quantified. Lymphatic ligation exacerbated beam walking deficits in SAH mice (Fig. 3E). Moreover, ligated mice showed lateral ventricle area enlargement post-SAH (Fig. 3F,G). Overall, these findings suggest that meningeal lymphatic drainage via dCLNs is crucial for early blood clearance post-SAH, and impaired MLV function aggravates pathology.

3.4 WBV Promotes Meningeal Lymphatic Drainage in SAH Mice

To investigate the impact of WBV on meningeal lymphatic drainage during SAH recovery, we performed real-

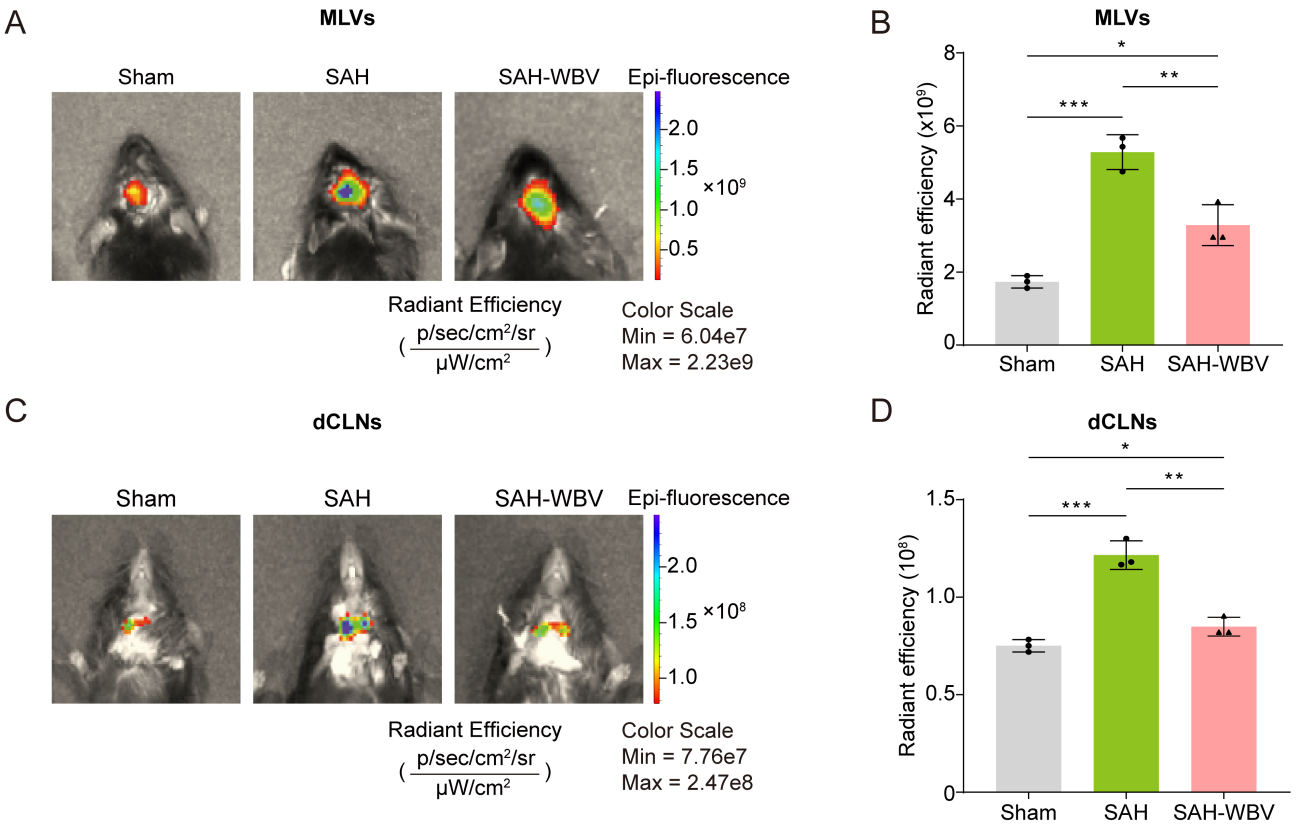

Fig. 4. WBV promotes meningeal lymphatic drainage in SAH mice. (A,B) Fluorescence intensity in MLVs 12 h post-intracerebroventricular injection of OVA-647 (5 μL). (C,D) Fluorescence intensity in dCLNs. Data are presented as mean ± SEM. Statistical significance: $*p < 0.05$, $**p < 0.01$, $***p < 0.001$. OVA-647, Alexa Fluor 647-conjugated ovalbumin.

time *in vivo* imaging by injecting OVA-647 (5 μL) into the lateral ventricle following a 3-week WBV intervention. Fluorescent signals were detected in MLVs and dCLNs 12 h post-injection. Quantitative analysis showed significantly higher fluorescence intensity in the periventricular and cervical regions of SAH mice compared to the sham group (Fig. 4A–D). Notably, WBV intervention decreased fluorescence intensity in both MLVs and dCLNs (Fig. 4A–D), suggesting that WBV enhanced macromolecule clearance via the MLVs and dCLNs.

3.5 WBV Promotes Meningeal Lymphangiogenesis

To explore the mechanisms underlying WBV-enhanced drainage, we assessed *Pdpn* and *Lyve-1* expression, lymphatic markers essential for valve development. The mRNA levels of *Pdpn* and *Lyve-1* were significantly upregulated in MLVs and dCLNs after WBV treatment in SAH mice (Fig. 5A,B). Consistently, the protein levels of PDPN and LYVE-1 were also increased in MLVs after WBV intervention (Fig. 5C,D; the original Western blot WB images can be found in the **Supplementary Materials-WB results**). Furthermore, immunofluorescence results showed that the LYVE-1-positive density and branching complexity of meningeal lymphatic vessels were increased in the SAH-WBV group compared to the SAH group (Fig. 5E–H). Overall, these findings indicate that WBV promotes meningeal lymphangiogenesis in MLVs and dCLNs.

3.6 WBV Increases the Peripheral $CD4^+Foxp3^+$ Treg Population and IL-10 Levels in SAH Mice

Tregs have been reported to promote tissue repair after neural injury [26]. Given that SAH recovery involves extensive tissue regeneration, we hypothesized that WBV might modulate Treg dynamics. To evaluate this hypothesis, we quantified the peripheral blood Treg population in mice after a three-week WBV intervention. Flow cytometry analysis revealed a significant increase in $CD4^+FoxP3^+$ Tregs post-SAH compared to sham controls, further enhanced by WBV treatment (Fig. 6A,B). As Treg cells primarily function through interleukin (IL)-10 secretion, we measured IL-10 levels in the sham, SAH, and SAH-WBV groups. Interestingly, IL-10 levels were significantly higher in the SAH group than in the sham control (Fig. 6C). Moreover, WBV treatment further increased IL-10 levels in SAH mice (Fig. 6C), consistent with the observed expansion of Treg cells in peripheral blood. These findings indicate that Treg expansion may be a mechanism underlying WBV-mediated neuroprotection.

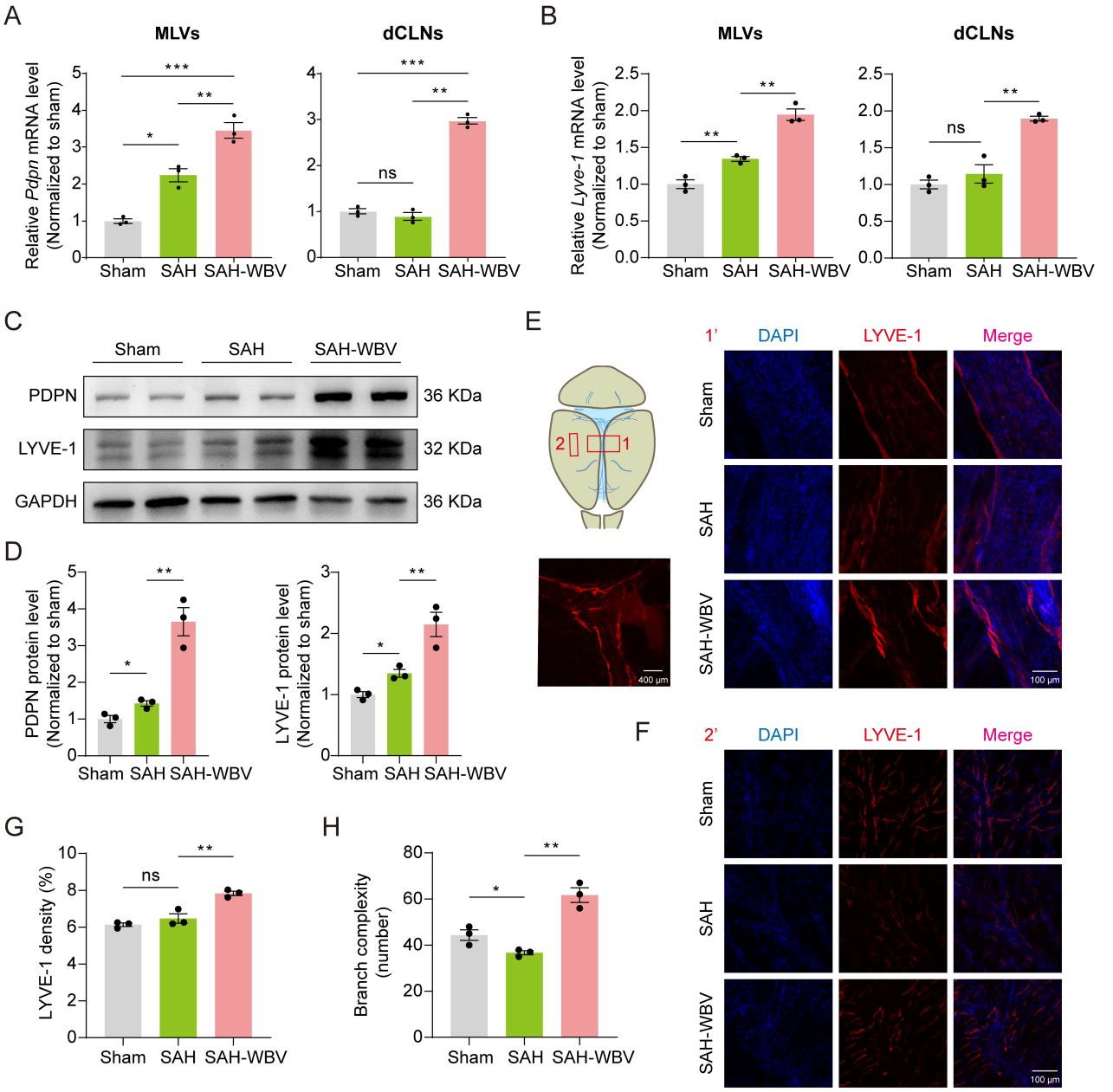

Fig. 5. WBV promotes meningeal lymphangiogenesis in SAH mice. (A,B) Relative *Pdpn* and *Lyve-1* mRNA levels in MLVs (A) and dCLNs (B). Normalized to sham (n = 3 mice/group; 3 technical replicates). (C,D) Relative PDPN and LYVE-1 protein levels in MLVs. (E,F) Representative images of staining for LYVE-1 in the MLVs of mice. Scale bar: 100 or 400 μm. (G,H) The LYVE-1-positive density and branch complexity in the MLVs. Data are presented as mean ± SEM. Statistical significance: ns, $p > 0.05$, *$p < 0.05$, **$p < 0.01$, ***$p < 0.001$. Lyve-1, lymphatic vessel endothelial hyaluronan receptor 1; Pdpn, podoplanin; DAPI, 4′,6-diamidino-2-phenylindole; GAPDH, glyceraldehyde-3-phosphate dehydrogenase.

4. Discussion

SAH is a severe cerebrovascular event accounting for only 5% of stroke but contributing to disproportionately high mortality [27]. Effective rehabilitation strategies remain urgently needed [28]. Our study demonstrates that WBV significantly improves long-term neurological recovery in a murine SAH model. Mechanistically, we identify two key therapeutic pathways: (1) improved MLV function and (2) modulation of peripheral immune responses through $CD4^+$ Tregs.

In this study, we used the widely accepted "blood injection" method to establish the SAH mouse model [29–31]. This model employed syngeneic donor blood. Although rigorous measures minimized donor-related vari-

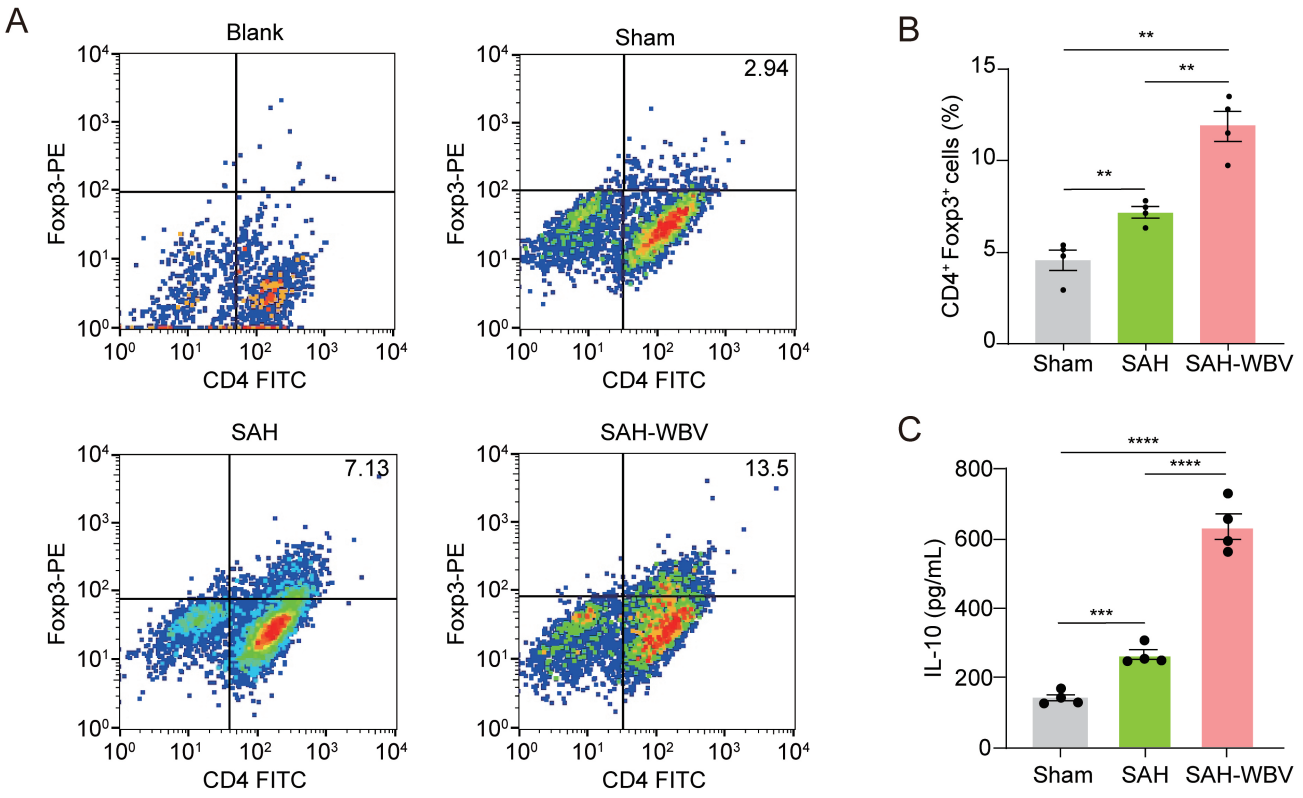

Fig. 6. WBV increases the peripheral CD4$^+$Foxp3$^+$ Treg population and IL-10 levels in SAH mice. (A) Flow cytometry of PBMCs: gated on CD4$^+$ Tregs. (B) Frequency of CD4$^+$Foxp3$^+$ cells (n = 4 independent experiments). (C) The IL-10 levels (n = 4). Data are presented as mean ± SEM. Statistical significance: $^{**}p < 0.01$, $^{***}p < 0.001$, $^{****}p < 0.0001$. IL, interleukin; CD4$^+$Foxp3$^+$, cluster of differentiation 4 and forkhead box protein P3 positive.

ability, a minor contribution of allogeneic factors to the inflammatory response cannot be entirely excluded. However, given the syngeneic donor background and consistent model application across groups, the primary pathophysiological outcomes and treatment effects reported are robust and valid.

The therapeutic potential of WBV in neurological disorders is attributed to its broad physiological effects, including improved in motor function, synaptic plasticity, and cognitive performance [17]. Notably, we demonstrated that WBV does not alter the population of CD4$^+$Foxp3$^+$ T cells or the MLV drainage capacity in sham mice (**Supplementary Fig. 1**), indicating that the observed Treg expansion and enhanced MLV drainage are specific to post-SAH recovery following WBV treatment. Our findings extend this evidence, showing that chronic WBV intervention alleviates SAH-induced deficits in motor coordination, spatial learning, and affective behavior. Although the Y-maze test showed limited sensitivity to WBV-induced changes, consistent improvements across multiple behavioral assessments highlight WBV's broad neurorestorative capacity. While our results demonstrate WBV's benefit in an SAH animal model, translating this intervention to acute SAH patients requires consideration. First, WBV's passive nature is a significant advantage. Critically ill SAH patients in neurointensive care unit are often sedated, ventilated, and have limited mobility [32]. WBV can be applied without active patient participation, benefiting those unable to engage in physical therapy. Second, modern, low-profile WBV platforms could be integrated into the intensive care unit (ICU). Patients could be transferred onto the platform for short, supervised sessions, minimizing disruption to monitoring and life support. Third, the primary concern in acute SAH is re-bleeding risk and elevated intracranial pressure (ICP) [33]. The feasibility of WBV hinges on the use of extremely low-magnitude, low-frequency vibrations. Furthermore, WBV parameters can be precisely controlled and titrated based on individual patient stability and real-time neuromonitoring. Fourth, the gentle muscular contractions induced by WBV could help maintain venous return, improve peripheral circulation, and preserve muscle tone, potentially reducing systemic complications. In summary, the application of WBV in acute SAH is a biologically plausible concept grounded in its potential to target key pathological pathways.

The discovery of MLVs has significantly advanced our understanding of brain waste clearance and immune surveillance [8]. Our findings reveal three key aspects of MLV function post-SAH: (1) MLVs actively mediate the early erythrocyte clearance from the subarachnoid space to

dCLNs, with erythrocyte congestion detectable in dCLNs within 1 h post-SAH; (2) improved MLV function correlates with neurological recovery; and (3) WBV enhances lymphatic regeneration and macromolecule drainage capacity. These observations align with emerging evidence highlighting the critical role of lymphatic drainage in regulating intracranial pressure, suggesting that WBV may expedite SAH recovery by enhancing this clearance pathway [23]. In this study, we demonstrated that WBV promotes meningeal lymphangiogenesis in MLVs and dCLNs and may be a mechanism underlying WBV-mediated protection. Importantly, WBV promotes meningeal lymphatic drainage through a multifactorial process primarily driven by the enhanced fluid dynamics and pulsatility. The mechanical oscillations from WBV are transmitted through the skeleton and vasculature to the cranium, acting as an external pulsatility source that synergizes with intrinsic arterial pulsations to augment CSF flow pumping forces [34]. This enhanced pulsatility facilitates the function of the glymphatic system by increasing para-arterial influx of CSF and the convective exchange of interstitial fluid, thereby delivering a greater volume of metabolic waste to the meningeal lymphatic vessels. Furthermore, the rhythmic mechanical deformation from vibration directly compresses and stimulates meningeal lymphatics, akin to how muscle contractions drive peripheral lymph flow, promoting the active propulsion of lymph towards the deep cervical lymph nodes [35]. Concurrently, WBV induces indirect physiological effects, such as modulating the autonomic nervous system toward a parasympathetic state that favors vasodilation and reducing systemic inflammation [36], which collectively create a more permissive environment for efficient glymphatic-lymphatic coupling and overall drainage capacity. Thus, WBV acts through a synergistic combination of direct mechanical pumping and optimized physiological conditions to significantly boost the function of the brain.

The immunomodulatory effects of WBV provide a novel mechanistic perspective. Our data reveal that WBV increases the peripheral $CD4^+Foxp3^+$ Treg population and may modulate neuroimmune communication through the meningeal lymphatic system. This observation significantly establishes a mechanistic link between Treg dysfunction and the pathophysiology of SAH. In addition, the enhanced meningeal lymphatic drainage and the expansion of Tregs may be mechanistically connected through a sequential process involving antigen transport and immune modulation. WBV enhances the pulsatile flow and functional capacity of meningeal lymphatic vessels. This improved drainage enables the efficient translocation of CNS-derived antigens from the cerebrospinal fluid to the dCLNs [37,38]. Within the immunologically active milieu of the dCLNs, these antigens are presented to naïve T cells. Given the tolerogenic environment typically induced by CNS-derived antigens to prevent autoimmune responses, this antigen presentation preferentially promotes the differentiation and clonal expansion of antigen-specific $Foxp3^+$ Tregs [39]. Thus, while WBV-induced enhancement of meningeal lymphatic function does not directly induce Treg expansion, it serves as a crucial upstream mechanism that delivers essential antigenic signals to the dCLNs, where the actual priming and amplification of immunosuppressive Tregs take place. This cascade ultimately supports neuroimmune homeostasis and contributes to recovery following SAH.

While our study provides insights into SAH recovery after WBV treatment, it is not without limitations. First, we focused on young male mice primarily to minimize potential confounding variables. By using a homogeneous cohort of young males, we aimed to establish a clear and robust baseline effect of SAH recovery under controlled experimental conditions. However, this choice is a limitation of our current study, and our findings may not be directly generalizable to females or older populations. Second, the beneficial effects of WBV observed in our study may not be solely due to direct neural effects but may also be mediated through systemic pathways, including cardiovascular and neuroendocrine responses. We hypothesize that these systemic changes could create a more favorable internal environment for neurorecovery, potentially reducing inflammation or promoting vascular health, which in turn supports neurological repair after SAH. In future studies, investigations specifically designed to correlate these hemodynamic and stress biomarkers with functional outcomes are essential and will be a critical next step to elucidate the precise mechanisms of WBV action.

5. Conclusions

In this study, we investigated the therapeutic potential of WBV, a non-pharmacological intervention, in a mouse model of SAH. Our results demonstrate that WBV treatment significantly improved cognitive function and motor performance in SAH-induced mice. Mechanistically, WBV enhanced the drainage capacity of MLVs to dCLNs and increased the population of peripheral Treg cells. In summary, our study identifies WBV as a promising non-invasive therapeutic strategy for SAH, based on its dual effects of enhancing meningeal lymphatic function and modulating immune responses. Given that the meningeal lymphatic system has emerged as a particularly promising target, it offers a novel pathway for innovative WBV-based interventions in the treatment of cerebrovascular diseases.

Availability of Data and Materials

All data reported in this paper will also be shared by the lead contact upon request.

Author Contributions

RX, YSS and XYT designed the research study. CYS, YYZ, XCS, JWC, SFL, XJL and XYT performed the re-

search. YYZ, SFL and XJL analyzed the data. YYZ, XCS, XYT and YSS wrote the manuscript. All authors contributed to editorial changes in the manuscript. All authors read and approved the final manuscript. All authors have participated sufficiently in the work and agreed to be accountable for all aspects of the work.

Ethics Approval and Consent to Participate

All animal experiments were conducted according to protocols approved by the Institutional Animal Care and Use Committee of Nanjing University (Ethic Approval Number: SY12), adhering to the Guide for Care and Use of Laboratory Animals of Nanjing University.

Acknowledgment

We gratefully acknowledge Jiang Chen (Nanjing University) for participating in valuable discussions.

Funding

This research was funded by the National Natural Science Foundation of China (82572130).

Conflict of Interest

The authors declare no conflict of interest.

Declaration of AI and AI-Assisted Technologies in the Writing Process

During the preparation of this work, the authors used ChatGPT-3.5 in order to check spelling and grammar. After using this tool, the authors reviewed and edited the content as needed and take full responsibility for the content of the publication.

Supplementary Material

Supplementary material associated with this article can be found, in the online version, at https://doi.org/10.31083/JIN49920.

References

[1] Hoh BL, Ko NU, Amin-Hanjani S, Chou SHY, Cruz-Flores S, Dangayach NS, *et al*. 2023 Guideline for the Management of Patients With Aneurysmal Subarachnoid Hemorrhage: A Guideline From the American Heart Association/American Stroke Association. Stroke. 2023; 54: e314–e370. https://doi.org/10.1161/STR.0000000000000436.

[2] Asada R, Suzuki H. Osteopontin in post-subarachnoid hemorrhage pathologies. Journal of Integrative Neuroscience. 2022; 21: 62. https://doi.org/10.31083/j.jin2102062.

[3] van Lieshout JH, Dibué-Adjei M, Cornelius JF, Slotty PJ, Schneider T, Restin T, *et al*. An introduction to the pathophysiology of aneurysmal subarachnoid hemorrhage. Neurosurgical Review. 2018; 41: 917–930. https://doi.org/10.1007/s10143-017-0827-y.

[4] van Gijn J, Kerr RS, Rinkel GJE. Subarachnoid haemorrhage. Lancet. 2007; 369: 306–318. https://doi.org/10.1016/S0140-6736(07)60153-6.

[5] Sherchan P, Lekic T, Suzuki H, Hasegawa Y, Rolland W, Duris K, *et al*. Minocycline improves functional outcomes, memory deficits, and histopathology after endovascular perforation-induced subarachnoid hemorrhage in rats. Journal of Neurotrauma. 2011; 28: 2503–2512. https://doi.org/10.1089/neu.2011.1864.

[6] Mashaly HA, Provencio JJ. Inflammation as a link between brain injury and heart damage: the model of subarachnoid hemorrhage. Cleveland Clinic Journal of Medicine. 2008; 75: S26–S30. https://doi.org/10.3949/ccjm.75.suppl_2.s26.

[7] Louveau A, Smirnov I, Keyes TJ, Eccles JD, Rouhani SJ, Peske JD, *et al*. Structural and functional features of central nervous system lymphatic vessels. Nature. 2015; 523: 337–341. https://doi.org/10.1038/nature14432.

[8] Ahn JH, Cho H, Kim JH, Kim SH, Ham JS, Park I, *et al*. Meningeal lymphatic vessels at the skull base drain cerebrospinal fluid. Nature. 2019; 572: 62–66. https://doi.org/10.1038/s41586-019-1419-5.

[9] Da Mesquita S, Fu Z, Kipnis J. The Meningeal Lymphatic System: A New Player in Neurophysiology. Neuron. 2018; 100: 375–388. https://doi.org/10.1016/j.neuron.2018.09.022.

[10] Pu T, Zou W, Feng W, Zhang Y, Wang L, Wang H, *et al*. Persistent Malfunction of Glymphatic and Meningeal Lymphatic Drainage in a Mouse Model of Subarachnoid Hemorrhage. Experimental Neurobiology. 2019; 28: 104–118. https://doi.org/10.5607/en.2019.28.1.104.

[11] Chen J, Wang L, Xu H, Xing L, Zhuang Z, Zheng Y, *et al*. Meningeal lymphatics clear erythrocytes that arise from subarachnoid hemorrhage. Nature Communications. 2020; 11: 3159. https://doi.org/10.1038/s41467-020-16851-z.

[12] Luo SQ, Gao SQ, Fei MX, Xue-Wang, Yan-Sun, Ran-Zhao, *et al*. Ligation of cervical lymphatic vessels decelerates blood clearance and worsens outcomes after experimental subarachnoid hemorrhage. Brain Research. 2024; 1837: 148855. https://doi.org/10.1016/j.brainres.2024.148855.

[13] Liu Q, Hou C, Zhang H, Fu C, Wang W, Wang B, *et al*. Impaired meningeal lymphatic vessels exacerbate early brain injury after experimental subarachnoid hemorrhage. Brain Research. 2021; 1769: 147584. https://doi.org/10.1016/j.brainres.2021.147584.

[14] Liao J, Zhang M, Shi Z, Lu H, Wang L, Fan W, *et al*. Improving the Function of Meningeal Lymphatic Vessels to Promote Brain Edema Absorption after Traumatic Brain Injury. Journal of Neurotrauma. 2023; 40: 383–394. https://doi.org/10.1089/neu.2022.0150.

[15] Gao D, Zou B, Zhu K, Bi S, Zhang W, Yang X, *et al*. Enhancing Th17 cells drainage through meningeal lymphatic vessels alleviate neuroinflammation after subarachnoid hemorrhage. Journal of Neuroinflammation. 2024; 21: 269. https://doi.org/10.1186/s12974-024-03252-y.

[16] Trans T, Aaboe J, Henriksen M, Christensen R, Bliddal H, Lund H. Effect of whole body vibration exercise on muscle strength and proprioception in females with knee osteoarthritis. The Knee. 2009; 16: 256–261. https://doi.org/10.1016/j.knee.2008.11.014.

[17] Cardoso ALBD, Sá-Caputo DC, Asad NR, van Heuvelen MJ, van der Zee EA, Ribeiro-Carvalho A, *et al*. Beneficial effects of whole-body vibration exercise for brain disorders in experimental studies with animal models: a systematic review. Behavioural Brain Research. 2022; 431: 113933. https://doi.org/10.1016/j.bbr.2022.113933.

[18] Wang Z, Sun C, Hu K, Zang Y, Cheng Y, Xu H, *et al*. Effects of whole-body vibration on animal models of neurodegenerative diseases: A systematic review. Experimental Neurology. 2026; 396: 115555. https://doi.org/10.1016/j.expneurol.2025.115555.

[19] Cariati I, Bonanni R, Pallone G, Romagnoli C, Rinaldi AM, Annino G, *et al*. Whole Body Vibration Improves Brain and Musculoskeletal Health by Modulating the Expression of Tissue-

Specific Markers: FNDC5 as a Key Regulator of Vibration Adaptations. International Journal of Molecular Sciences. 2022; 23: 10388. https://doi.org/10.3390/ijms231810388.

[20] Oroszi T, Huiting W, Keijser JN, Nyakas C, van Heuvelen MJG, van der Zee EA. Whole-Body Vibration Affects Hippocampal Choline Acetyltransferase and Synaptophysin Expression and Improves Spatial Memory in Young Adult Mice. Journal of Integrative Neuroscience. 2024; 23: 173. https://doi.org/10.31083/j.jin2309173.

[21] Zhao L, He LX, Huang SN, Gong LJ, Li L, Lv YY, *et al*. Protection of dopamine neurons by vibration training and up-regulation of brain-derived neurotrophic factor in a MPTP mouse model of Parkinson's disease. Physiological Research. 2014; 63: 649–657. https://doi.org/10.33549/physiolres.932743.

[22] Boerema AS, Heesterbeek M, Boersma SA, Schoemaker R, de Vries EFJ, van Heuvelen MJG, *et al*. Beneficial Effects of Whole Body Vibration on Brain Functions in Mice and Humans. Dose-Response. 2018; 16: 1559325818811756. https://doi.org/10.1177/1559325818811756.

[23] Moreira-Marconi E, Teixeira-Silva Y, Meirelles AGD, Melo-Oliveira MEDS, Santos ACG, Reis-Silva A, *et al*. Inflammatory Biomarker Responses to Whole-Body Vibration in Subjects with Different Clinical Status: A Systematic Review. International Journal of Environmental Research and Public Health. 2022; 19: 14853. https://doi.org/10.3390/ijerph192214853.

[24] Sabri M, Ai J, Macdonald RL. Dissociation of vasospasm and secondary effects of experimental subarachnoid hemorrhage by clazosentan. Stroke. 2011; 42: 1454–1460. https://doi.org/10.1161/STROKEAHA.110.604728.

[25] Teng XY, Hu P, Zhang CM, Zhang QX, Yang G, Zang YY, *et al*. OPALIN is an LGI1 receptor promoting oligodendrocyte differentiation. Proceedings of the National Academy of Sciences of the United States of America. 2024; 121: e2403652121. https://doi.org/10.1073/pnas.2403652121.

[26] Shi L, Sun Z, Su W, Xu F, Xie D, Zhang Q, *et al*. Treg cell-derived osteopontin promotes microglia-mediated white matter repair after ischemic stroke. Immunity. 2021; 54: 1527–1542.e8. https://doi.org/10.1016/j.immuni.2021.04.022.

[27] Neifert SN, Chapman EK, Martini ML, Shuman WH, Schupper AJ, Oermann EK, *et al*. Aneurysmal Subarachnoid Hemorrhage: the Last Decade. Translational Stroke Research. 2021; 12: 428–446. https://doi.org/10.1007/s12975-020-00867-0.

[28] Ikram A, Javaid MA, Ortega-Gutierrez S, Selim M, Kelangi S, Anwar SMH, *et al*. Delayed Cerebral Ischemia after Subarachnoid Hemorrhage. Journal of Stroke and Cerebrovascular Diseases. 2021; 30: 106064. https://doi.org/10.1016/j.jstrokecerebrovasdis.2021.106064.

[29] Chen P, Liu XY, Lin MH, Li YX, Kang DZ, Ye ZC, *et al*. NeuroD1 administration ameliorated neuroinflammation and boosted neurogenesis in a mouse model of subarachnoid hemorrhage. Journal of Neuroinflammation. 2023; 20: 261. https://doi.org/10.1186/s12974-023-02949-w.

[30] Nakagawa R, Itokazu T, Shibuya N, Kishima H, Yamashita T. Perivascular Neutrophil Extracellular Traps Exacerbate Microvasospasm After Experimental Subarachnoid Hemorrhage. Stroke. 2024; 55: 2872–2881. https://doi.org/10.1161/STROKEAHA.124.047574.

[31] Tan X, Li X, Li R, Meng W, Xie Z, Li J, *et al*. β-hydroxybutyrate alleviates neurological deficits by restoring glymphatic and inflammation after subarachnoid hemorrhage in mice. Experimental Neurology. 2024; 378: 114819. https://doi.org/10.1016/j.expneurol.2024.114819.

[32] Schmidbauer ML, Wiegand TLT, Keidel L, Zibold J, Dimitriadis K. Intrahospital Transport of Critically Ill Patients with Subarachnoid Hemorrhage-Frequency, Timing, Complications, and Clinical Consequences. Journal of Clinical Medicine. 2023; 12: 7666. https://doi.org/10.3390/jcm12247666.

[33] Hov MR, Ryen A, Finsnes K, Storflor J, Lindner T, Gleditsch J, *et al*. Pre-hospital ct diagnosis of subarachnoid hemorrhage. Scandinavian Journal of Trauma, Resuscitation and Emergency Medicine. 2017; 25: 21. https://doi.org/10.1186/s13049-017-0365-1.

[34] Jindrak KF, Jindrak H. Mechanical effect of vocalization on human brain and meninges. Medical Hypotheses. 1988; 25: 17–20. https://doi.org/10.1016/0306-9877(88)90040-0.

[35] Inês Gonzáles A, Lavarda do Nascimento G, da Silva A, Bernardo-Filho M, da Cunha de Sá-Caputo D, Sonza A. Whole-body vibration exercise in the management of cardiovascular diseases: A systematic review. Journal of Bodywork and Movement Therapies. 2023; 36: 20–29. https://doi.org/10.1016/j.jbmt.2023.04.057.

[36] Jalilian H, Zamanian Z, Gorjizadeh O, Riaei S, Monazzam MR, Abdoli-Eramaki M. Autonomic Nervous System Responses to Whole-Body Vibration and Mental Workload: A Pilot Study. The International Journal of Occupational and Environmental Medicine. 2019; 10: 174–184. https://doi.org/10.15171/ijoem.2019.1688.

[37] Kovacs MA, Cowan MN, Babcock IW, Sibley LA, Still K, Batista SJ, *et al*. Meningeal lymphatic drainage promotes T cell responses against *Toxoplasma gondii* but is dispensable for parasite control in the brain. eLife. 2022; 11: e80775. https://doi.org/10.7554/eLife.80775.

[38] Hsu M, Rayasam A, Kijak JA, Choi YH, Harding JS, Marcus SA, *et al*. Neuroinflammation-induced lymphangiogenesis near the cribriform plate contributes to drainage of CNS-derived antigens and immune cells. Nature Communications. 2019; 10: 229. https://doi.org/10.1038/s41467-018-08163-0.

[39] Berghoff AS, Kresl P, Rajky O, Widhalm G, Ricken G, Hainfellner JA, *et al*. Analysis of the inflammatory tumor microenvironment in meningeal neoplasms. Clinical Neuropathology. 2020; 39: 256–262. https://doi.org/10.5414/NP301156.